Journal of Zhejiang University-SCIENCE A (Applied Physics & Engineering)
ISSN 1673-565X (Print); ISSN 1862-1775 (Online)
www.jzus.zju.edu.cn; www.springerlink.com
E-mail: jzus@zju.edu.cn

Numerical analysis of reasons for the CO distribution in an opposite-wall-firing furnace

Xiao-qiang XIE[1], Jian-guo YANG[†‡1], Chao-yang ZHU[2], Chuan-huai LIU[2], Hong ZHAO[1], Zhi-hua WANG[1]

[1]*State Key Laboratory of Clean Energy Utilization, Zhejiang University, Hangzhou 310027, China*

[2]*Huaizhe Coal & Power Fengtai Power Co., Ltd., Huainan 232131, China*

[†]E-mail: yjg@zju.edu.cn

Received July 31, 2019; Revision accepted Jan. 13, 2020; Crosschecked Feb. 10, 2020

Abstract: In practical operations, the carbon monoxide (CO) distribution in an opposite-wall-firing furnace (OWFF) is characterized by a high concentration near the side walls and a low concentration in the center, accompanied by a series of combustion-related issues. To find the reasons for the CO distribution, a numerical study was conducted on a 660 MWe OWFF. The CO concentration profiles, distribution coefficients of coal and air, mixing coefficients, and the aerodynamic characteristics were extracted for analysis. The CO distribution within the furnace greatly depends on the mixing of coal and air. A mismatch between the aerodynamic behaviors of coal and air causes the non-uniform distribution of CO. Taking into consideration that distinctive flow patterns exist within the different regions, the formation mechanisms of the CO distribution can be divided into two components: (1) In the burner region, the collision of opposite flows leads to the migration of gas and particles toward the side wall which, together with the vortexes formed at furnace corners, is responsible for unburned particles concentrated and oxygenized from the furnace center to the side wall. Thus, high CO concentrations appear in these areas. (2) As the over-fire air (OFA) jet is injected into the furnace, it occupies the central region of furnace and pushes the gas from the burner region outward to the side wall, which is disadvantageous for the mixing effect in the side wall region. As a consequence, a U-shaped distribution of CO concentration is formed. Our results contribute to a theoretical basis for facilitating the control of variation in CO concentration within the furnace.

Key words: Opposite-wall-firing furnace (OWFF); Carbon monoxide (CO) distribution; Distributions of coal and air; Gas/particle flow; Corner vortex; Over-fire air (OFA)

https://doi.org/10.1631/jzus.A1900363 **CLC number:** TK224.1

1 Introduction

The opposite-wall-firing furnace (OWFF) is one of the most widely used types of furnaces for coal-fired plants, because of its removal of gas temperature deviation at the furnace exit and maintenance of stable combustion at minimum loads (Liu et al., 2013). As the combustion process differs greatly for furnaces with different firing systems, the OWFF exhibits many special features in operation. One of those is the U-shaped distribution of carbon monoxide (CO) across the width of the furnace. That is, the CO concentration is high near the side walls but low in the middle of the furnace, and the difference is large (Hong et al., 2012; Yang et al., 2015; Xie et al., 2019). Over the past decade, coal-fired plants have been required to be equipped with low nitrogen oxide (NO_x) combustion technologies to meet increasingly stringent emission standards. The main principle of these technologies is the staging of fuel and air, which produces a sequence of local fuel-rich and fuel-lean zones inside the furnace. Thus, without good

‡ Corresponding author
ORCID: Xiao-qiang XIE, https://orcid.org/0000-0001-8834-354X; Jian-guo YANG, https://orcid.org/0000-0002-3070-5111

aerodynamic fields organized in the whole furnace, the variation in CO concentration will be exacerbated.

Like other coal-fired furnaces, OWFFs are vulnerable to the problems of low boiler efficiency, high NO_x emission, severe slagging, and high temperature corrosion when low NO_x combustion technology is employed. Note that all these problems are pertinent to one parameter, the CO distribution within the furnace: (1) CO is the main product of inadequate burning of fuel, and the maldistribution of CO is a reflection of non-uniform combustion, which results in the degradation of boiler efficiency (Bar-Ziv et al., 2014); (2) areas of high CO concentration in the furnace are favorable for the reduction of NO_x (van der Lans et al., 1997), and thus the ultimate NO_x emission varies with different CO distributions; (3) the enrichment of CO in the vicinity of the water walls is conducive to the formation of strongly reducing atmospheres, accelerating both slagging (Chen et al., 2017) and high temperature corrosion (Yang et al., 2017). It is necessary to study the CO distribution in the furnace and its associated causes to enable better boiler performance in terms of low NO_x emissions, high boiler efficiency, a low propensity for slagging, and resistance to high temperature corrosion, especially for an OWFF.

The CO distribution in the furnace is correlated with a number of factors, such as coal properties (combustion characteristics, particle size), the gas/particle flow field near the burner, the area of expansion and the penetration depth of the over-fire air (OFA) jet, and the overall gas/particle flow pattern throughout the furnace. With regard to OWFFs, both experimental and numerical studies have been performed to gain partial insights into the interplay between these factors and the lateral CO distribution characteristics within the furnace. Li et al. (2002) and Chen et al. (2008) carried out a series of model-scale gas/particle two-phase flow tests on a wide range of swirl burners, in conjunction with a phase Doppler anemometer facility. They concluded that a moderate recirculation zone in the near-burner-region, combined with appropriate variation in the type of particle concentration in the primary air duct, is beneficial for major particles gathered in the recirculation zone, reducing particles thrown to, and burning near, the side wall, hence an oxidizing atmosphere forms in the side wall region. Subsequent industrial combustion trials have proven this finding (Li et al., 2008, 2014; Chen et al., 2011). Zhou et al. (2014) conducted a similar two-phase experiment with an HT-NR3 swirl burner, and found that the unique distributions of gas/particle flows delay the mixing of primary air (PA) with secondary air (SA), resulting in a poor burnout of pulverized-coal (PC). The unburned particles are inclined to reach the side wall by penetrating SA, which compounds the reducing atmosphere there. Vikhansky et al. (2004) used a computational fluid dynamics (CFD) code GLACIER to investigate the mixing capacity of air and flue gases in the burnout zone of a 550 MWe OWFF with a staggered layout of OFA ports. They demonstrated that a higher penetration depth can enhance the coverage of OFA, which eventually guarantees a better reburning of CO. Liu et al. (2013) presented a simulation of a 600 MWe OWFF. The distribution of CO indicated that the CO generated at the center of the flame zone is pushed to the side wall after colliding at the center of the burner zone. The flue gas with a high CO concentration moves upward near the side wall, and will not mix with OFA. Yang et al. (2015) numerically diagnosed the combustion processes in two 500 MWe OWFFs, and found that the shape of low oxygen (O_2) areas along the side wall can be explained by the influence of the OFA. A large OFA flow rate creates narrow low O_2 areas along the side wall. In addition, low O_2 areas can be traced to particular burners, so adjusting the air supply to these burners may balance the CO profiles. This was verified in engineering practice (Purimetla and Cui, 2009; Hong et al., 2012; Liu et al., 2018; Xie et al., 2019). Despite these studies, the spatial distributions of coal and air, and the related mixing characteristics inside the furnace, which are essential to understanding the process of formation of the CO distribution, are largely unknown and need further research.

Experiments, ranging from scaled down model tests (He et al., 2005; Fan et al., 2010) to full-scale furnace tests (Costa and Azevedo, 2007; Li et al., 2008), are frequently used to reveal the aerodynamic and combustion behaviors of furnaces. However, these experiments are restricted not only by the amount of labor and expense required, but also by the application conditions of the instruments needed.

Moreover, only limited data is available from the experiments, and it contains much uncertainty.

In contrast, CFD constitutes an outstanding tool for giving continuous and accurate portrayals of various variables. As the calculating power and mathematical models are being constantly improved, numerical simulations have been extensively applied to coal-fired furnaces for the visualization of the combustion processes. Numerical studies on OWFFs have covered many aspects, including oxy-fuel combustion, biomass co-firing, utilization of low rank coal, slagging, high temperature corrosion, NO_x reduction, and combustion diagnosis and optimization (Vuthaluru and Vuthaluru, 2006; Choi and Kim, 2009; Liu et al., 2013).

In this study, a numerical simulation was performed on a 660 MWe OWFF, with the aim of investigating the causes of the U-shaped distribution of CO concentration across the width of the furnace. The adopted models and the relevant parameters were validated by comparing the simulation results with measured and design values. Attention was focused on the CO concentration profiles, the distribution coefficients of coal and air, the mixing coefficients, and the aerodynamic characteristics in different parts of the furnace. The obtained results can be applied to identify the root causes behind the CO distribution within the furnace. This knowledge can then be used to accelerate improvements in operational strategies and combustion system amelioration in this type of furnace.

2 Methodology

2.1 Opposite-wall-firing furnace

The furnace in this study was a Π type 660 MWe supercritical unit comprising an opposite firing system with swirl burners. Fig. 1a presents a schematic view of the furnace. The nominal dimensions of the furnace are approximately: height 66.7 m, width 19.4 m, and depth 15.5 m. The firing system is made up of 36 nozzles: 24 burners and 12 OFA ports. On each of the front and rear walls, 12 burners are arranged symmetrically, with four in a row by three different levels. The burner consists of three annular inlets. Through the central channel of the burner, the PA with PC is injected into the furnace in the form of an axial flow. The SA is divided into non-swirling inner secondary air (ISA) and swirling outer secondary air (OSA), introduced by the inner and outer annuli of the burner, respectively. Above the burners, there are another two levels of OFA ports. The upper one contains eight main OFA ports, aligned perpendicular to the burner columns, whereas the lower one contains four side OFA ports, close to the side walls. The main OFA jet is composed of three air streams. The central stream is an axial flow while both the inner and outer streams are swirl flows. The swirls in the inner and outer air have an identical direction. The side OFA jet is composed of only two air streams: the central air without swirling and the outer air with swirling. The precise position and swirl direction of each nozzle are indicated in Fig. 1b.

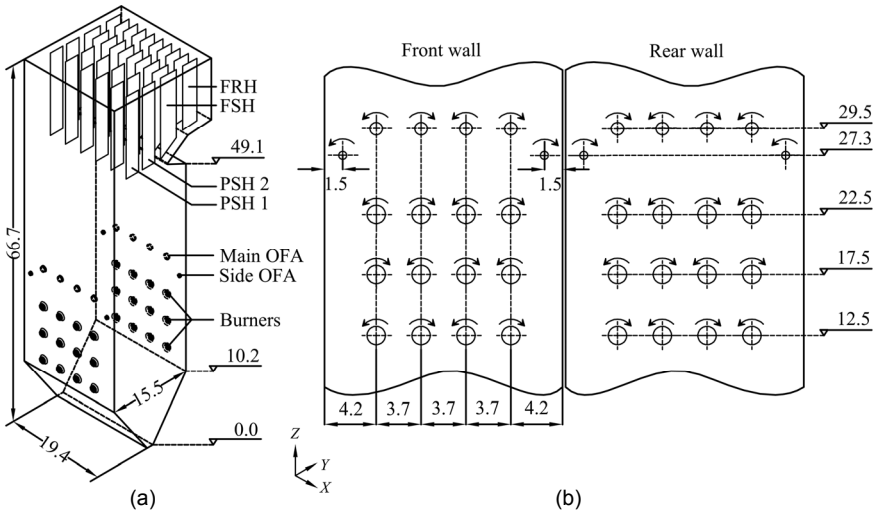

Fig. 1 Configuration of the furnace (unit: m): (a) geometry; (b) layout of the nozzles
FRH: final reheater; FSH: final superheater; PSH: platen superheater

2.2 Operational condition

The case under consideration was the full load condition, since it features the lowest overall stoichiometry ratio with the most significant difference in CO levels between the side wall region and the central region. Typical parameters for the full load run of the boiler are summarized in Table 1, and the physical and chemical properties of the coal involved are listed in Table 2. The PA accounts for 23%, SA for 54%, and OFA for 20% of the total air intake. The remaining 3% represents the overall air leakage into the furnace through the bottom ash hopper (Karampinis et al., 2012; Szuhánszki et al., 2013). At full load, only five of the six rows of burners are in operation. Normally, the upper burners on the rear wall are set to standby in case of emergency situations. From the inoperative burner, although no PA or PC is injected, a small amount of SA is supplied for cooling, which is assumed to be 30% of that assigned to the active burner (Drosatos et al., 2016). The PA/PC mixture enters the furnace at a temperature of 348 K, while the SA and OFA are preheated to 618 K. The size distribution of PC (Table 2) was derived from samples before entry into burners. A Rosin-Rammler function (Rosin and Rammler, 1933) was then fitted to the sieve data and employed for the following simulation. The size of PC varied between 1 and 250 μm, and the mean diameter was calculated to be 55 μm with a spread parameter of 1.1.

2.3 Calculation domain and mesh system

Fig. 2 is a diagram of the calculation domain and the grid system, as implemented for the present study. The domain of interest extends from the ash hopper to the outlet of final reheater, and incorporates burners, OFA ports, platen superheaters (PSHs 1 and 2 in Fig. 1a), a final superheater (FSH in Fig. 1a), and a final reheater (FRH in Fig. 1a). For the most reliable prediction of combustion phenomena, the simulated domain, in principle, should be created as close to the original furnace geometry as possible. However, it is impossible to rebuild the complete structures of an industrial furnace in a practical CFD trial. To make a proper compromise between computational resources and numerical accuracy, simplifications of the furnace construction were made. Half of the furnace was modeled based on the geometric symmetry and the nozzles of two half parts rotating in opposite directions (Huang et al., 2006; Park et al., 2013; Szuhánszki et al., 2013). The superheater and reheater panels in the upper part of the furnace were approximated as thin walls, whilst the number of panels was reduced. A simplified nozzle geometry was also introduced, given that there was a large discrepancy in scale between the furnace chamber and the nozzles. For all nozzles, the swirl vanes were neglected and the length of the air duct shortened. Furthermore, regarding burners, the flame stabilizing gears at the spout of the PA duct were not taken into account.

Table 1 Main operational parameters of the boiler

Parameter	Value
Total coal feed rate (kg/s)	71.0
Flow rate of PA (kg/s)	133.4
PA/PC mixture temperature (K)	348
Flow rate of SA (kg/s)	313.2
SA/OFA temperature (K)	618
Rear wall upper four burners coal feed rate (kg/s)	0
Rear wall upper four burners PA mass flow (kg/s)	0
Rear wall upper four burners SA mass flow (kg/s)	17.7
Flow rate of OFA (kg/s)	116
Flow rate of leakage air (through hopper) (kg/s)	17.4

Table 2 Coal properties

Parameter		Value
Proximate analysis (in weight, as received) (%)	Fixed carbon	28.00
	Volatiles	39.00
	Moisture	7.00
	Ash	26.00
Ultimate analysis (in weight, as received) (%)	Carbon (C)	56.37
	Hydrogen (H)	3.72
	Oxygen (O)	5.54
	Nitrogen (N)	1.00
	Sulfur (S)	0.37
Coal size distribution before burners (in weight) (%)	Residue on 90 μm sieve	17.93
	Residue on 200 μm sieve	1.60
Net heating value (as received) (MJ/kg)		21.30
Density (kg/m^3)		1300

A partition meshing method was employed for the discretization of furnace volume, and the developed grid (Fig. 2) comprising 913 034 hexahedral

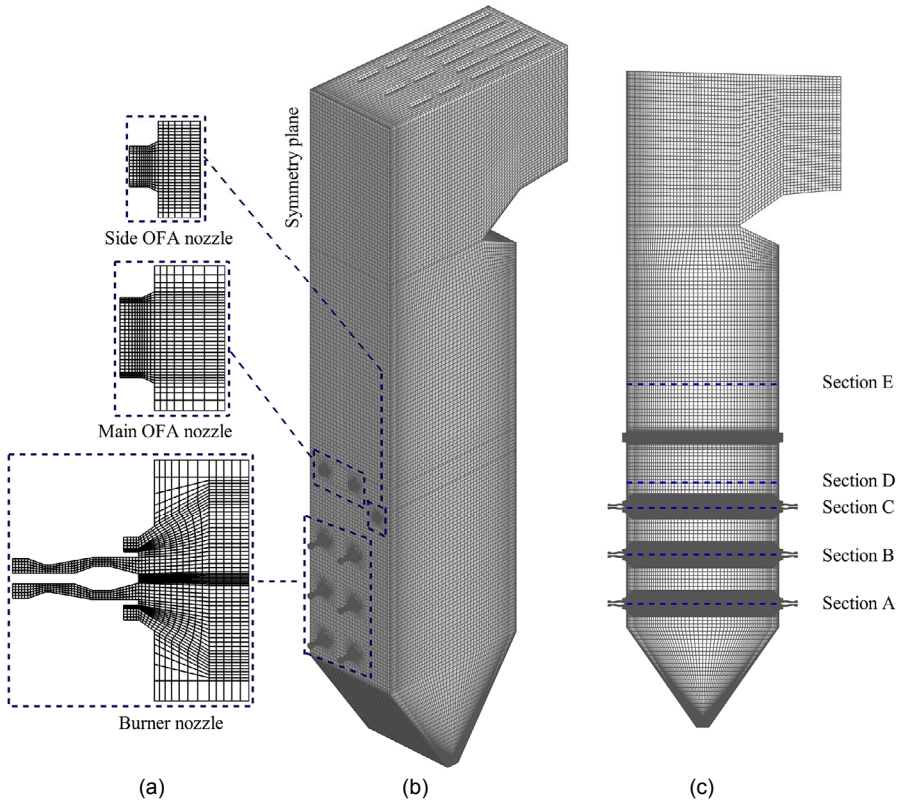

Fig. 2 Mesh constructed for: (a) the burner and OFA nozzles; (b) the furnace; (c) the vertical cross-section through the burners

cells. The mesh was locally refined in the neighborhood of the burner, OFA ports, and in the near-wall-region where sharp changes of flow field and temperature were expected. The grid at the burner exit was patched parallel to the jet direction (Fig. 2a) to eliminate the pseudo-diffusion problem caused by the flow being oblique to the grid lines (Xu et al., 1998). The sensitivity of the grid was tested using two additional sets of mesh, consisting of 767 304 and 1 407 076 cells, respectively. The distribution of the mass-weighted average gas temperature along the furnace height and the gas properties at the furnace exit were used as validation criteria. Similar performances were observed from the 913 034 cells and 1 407 076 cells, so the current grid system was confirmed as grid-independent.

2.4 Numerical models

A numerical simulation was performed using the commercial CFD software ANSYS FLUENT V.16.0. The flow was modeled in a Eulerian frame where the time-averaged conservation equations for mass, momentum, enthalpy, and species (mass fraction) are solved with the SIMPLE algorithm for pressure correction. The realizable k-ε model (Shih et al., 1995) was selected to close the turbulence terms of these equations, on account of its better description of the recirculation zone located downstream from the swirl burner. The flow-wall effect was handled by the standard wall function to attain stable calculation and fast convergence. In contrast to the fluid, coal particles were tracked in a Lagrangian scheme. The motion of particles was determined from the force balance, whereas the dispersion was predicted by the stochastic tracking model with a statistically sufficient number of particles modeled simultaneously. Here, this number was taken to be 10. The coupling of mass, momentum, energy, and species between phases was incorporated as the source/sink terms in the respective governing equations. Particle size has an important impact on realistic particle behavior. To consider such an effect, the PC was segmented into 10 distinct size classes, obeying the Rosin-Rammler distribution, as analyzed in Section 2.2.

As coal particles proceed in the furnace, they undergo devolatilization and char combustion in sequence. The two-competing rate model proposed by Kobayashi et al. (1977) was adopted for the devolatilization mechanism, which assumes volatile release is dependent on particle temperature, whilst the reaction rates of two parallel first order reactions, expressed in Arrhenius forms, are weighted to obtain the yield rate of volatiles. The composition of volatiles was derived from the proximate and ultimate analyses of coal presented in Table 2, based on the hypothesis that the char is composed solely of carbon (Vuthaluru and Vuthaluru, 2006). Heterogeneous char combustion was calculated according to the kinetic/diffusion limited model of Field (1969) and Baum and Street (1971), supposing that the oxidation rate of residual char is controlled by both the external diffusion of O_2 to the surface and the internal chemical reactivity. The detailed parameters used to quantify the devolatilization and char combustion processes are given in Table 3. The coal particles were approximated as having a spherical shape and a constant diameter with their density decreasing while travelling throughout the furnace (Fan et al., 1999). The initial density of a particle was set to 1300 kg/m^3. Homogeneous gaseous reaction was computed using the non-premixed combustion concept. The concept states that the chemical reaction is infinitely fast compared with the mixing rate so that chemical equilibrium can be assumed for the gas phase. The mass fraction of individual species was determined by a single mixture fraction under the assumption that all gaseous species have a common diffusion rate, which is a proper approximation for the turbulent flow. Turbulence-chemistry interactions were accounted for by the fraction variance together with the probability density function (PDF) (Sivathanu and Faeth, 1990). Huang et al. (2006) proved that the non-premixed combustion model can give satisfactory prediction of CO for engineering purposes and so was acceptable for the present work.

Radiation is the dominant heat transfer mechanism in the furnace, and was simulated using the P1 model (Cheng, 1964) due to the large optical thickness in industrial furnace cases. The domain-based weighted-sum-of-gray-gases model (WSGGM) (Smith et al., 1982) was applied for the calculation of the absorption coefficient of the gas mixture, while a constant value of 0.15 was accepted for the gaseous scatter coefficient. The particle emissivity was specified as 0.9, and the scatter coefficient as 0.6.

Table 3 Parameters for calculating the devolatilization and char combustion rates

Parameter	Value	
	Step 1	Step 2
Devolatilization		
Weighting factor	0.3	1
Pre-exponential factor (s^{-1})	3.7×10^5	1.5×10^{13}
Activation energy (J/mol)	7.4×10^4	2.5×10^5
Char combustion		
Diffusion constant	5×10^{-12}	
Pre-exponential factor (s/m)	0.002	
Activation energy (J/mol)	7.9×10^4	

2.5 Boundary conditions

The inlet conditions for the current case were extracted from industrial-scale measurement, and the average air distributions to each type of nozzle are provided in Table 4. The fuel particles were assumed to be injected at the same velocity as the PA, and all the fuel and air streams were split evenly across the relevant nozzles. Special care was given to the inlet settings of swirl flow, aiming to compensate for the omission of swirl vanes. Preliminary calculations were carried out on a single burner with different vane angles, and the swirl numbers of OSA, defined as the ratio of tangential momentum flux to axial momentum flux, were exported to determine the input condition of the burner's OSA inlet in full furnace simulation (Vikhansky et al., 2004; Park et al., 2013; Yang et al., 2015). Note that the structure of the swirl generator of the OFA ports was similar to that of the burners, and the swirl numbers of OSA were also applied to other rotatory jets (Table 4). The swirl part of each nozzle was modeled in a local cylindrical coordinate system, using the normal and tangential components of velocity.

For the wall conditions, the temperature of the working medium inside each heat exchanger, i.e. the water-cooled walls, superheaters, and reheaters, was set to the average of the respective inlet and outlet values. The effective heat transfer coefficient of each

section was recalculated based on the heat absorption data drawn from the thermodynamic analysis, while a typical emissivity value of 0.7 was imposed on all the wall surfaces.

Table 4 Run parameters of the burner, main OFA port, and side OFA port at full load

Parameter	Value		
	Burner	Main OFA port	Side OFA port
Mass flow rate of coal (kg/s)	3.55	–	–
Mass flow rate of primary air/central air (kg/s)	6.67	3.92	1.77
Mass flow rate of inner secondary air/inner air (kg/s)	2.81	6.54	–
Vane angle of inner air (°)	–	45	–
Swirl number of inner air	–	0.41	–
Mass flow rate of outer secondary air/outer air (kg/s)	11.97	1.43	3.45
Vane angle of outer secondary air/outer air (°)	45	45	90
Swirl number of outer secondary air/outer air	0.41	0.41	0

2.6 Mixing characteristics

To investigate the mixing characteristics of PC and air in the gas-solid reacting flow, a specific post-processing procedure was undertaken. The horizontal cross-sections, at 25.2 and 35.2 m, marked by sections D and E in Fig. 2, were chosen as the planes for analysis. Section D was referred to as the outlet of the burner region, and section E as the outlet of the OFA region. The gas variables on these cross-sections could be used to feature the ongoing combustion phenomena within the correspondent region. Each cross-section was divided into 400 ($i\times j$) facets, with 16 (i) and 25 (j) segments evenly spaced in the width and depth directions, respectively. The coordinate origin was set in the furnace center; the distance to the origin was denoted as X along the width direction and as Y along the depth direction. The key issue is the spatial distributions of coal and air. The weight loss of particles and the conversion of gas species during the combustion process compound the difficulties of identifying the mixing characteristics of coal and air. To solve these problems, coal particles were tracked on the basis of a converged reacting flow field whilst the interaction with the continuous phase was disabled. The initial mass flow of particles, before participating in combustion, for each facet was calculated. Molecular nitrogen was selected as the air tracer, because the nitrogen generated by the coal combustion is less than 0.1% of that carried in the combustion air. In this way, the localized degree of mixing between coal and air can be quantified without having to consider the influence of combustion on the mass change of particles and gas. The coal distribution coefficient η_p, air distribution coefficient η_a, and mixing coefficient η were defined as

$$\eta_p = \frac{M_{p,i,j}}{M_p}, \tag{1}$$

$$\eta_a = \frac{M_{n,i,j}}{M_n}, \tag{2}$$

$$\eta = \frac{\eta_p}{\eta_a}, \tag{3}$$

where $M_{p,i,j}$ is the initial particle mass flow rate crossing the (i, j) facet, kg/s; M_p is the initial particle mass flow rate at the whole cross-section, kg/s; $M_{n,i,j}$ is the nitrogen mass flow rate through the (i, j) facet, kg/s; M_n is the global nitrogen mass flow rate integrated over the whole cross-section, kg/s.

3 Results and discussion

3.1 Validation of the CFD model

To confirm the validity of the model setup as described, the predicted gas properties at the furnace exit (the position between the FSH and FRH sections) were compared with the design values and the experimental data for the full load condition (Table 5). The numerical results in Table 5 are the mass-weighted averaged values over the furnace exit plane. As there was no measuring port at the furnace exit, the flue gas was sampled through 14 ports at the exit of the economizer. Seven of those ports were arranged equidistantly along the horizontal direction on both of the left and right parts of the economizer. The gas composition was analyzed in situ by a Madur GA-21 Plus instrument with measurement ranges of 0–25% (in volume) for O_2, and 0–2% for CO. The relative errors of the analyzer were 2% for O_2 and 5% for CO. Generally, flue gas is not uniformly distributed along

a measuring probe. For more accurate measurement, a multipoint sampling principle was followed at each port. The recorded O_2 concentration value in Table 5 is an average of the 14 ports at the economizer exit. The numerical and experimental results coincided well, with a maximum discrepancy of 4.5% for the excess O_2 content (Table 5).

The objective of the simulation was to find the reason for the characteristic in-furnace CO distribution along the furnace width. A port-to-port comparison between the predicted CO profiles at the furnace exit and those monitored at the economizer exit is plotted in Fig. 3. It must be stressed that the CO concentrations collected from only the right ports of the economizer were used for comparison because only half of the furnace was considered for the present study. To lessen the experimental errors in relation to the positions of the measuring probes, the average values in the areas nearby the probes were calculated. Both curves followed an identical tendency along the furnace width: the CO concentration was dense near the side wall and sparse in the center of the furnace, giving the so-called "U-shaped profile of CO concentration." However, the numerical and measured CO volume fractions (on a dry basis) showed clear deviations, especially in the range of X between 3.7 and 9.7 m. Specifically, the measured CO concentration increased rapidly about 6 m away from the side wall, whereas a sharp increase of the calculated values was perceptible only within 2 m of the side wall. The difference was mainly attributable to the continuous process of gaseous turbulent diffusion along the flow path between the furnace exit and the economizer exit. From an engineering perspective, the numerical results gave a reasonable representation of the realistic combustion behavior of the furnace, therefore supporting the feasibility of the model established for the current problem.

3.2 Distribution characteristics of CO concentration along the furnace width

Detailed information in regard to the horizontal CO distributions within the furnace is presented in Fig. 4. Large amounts of CO accumulated in the vicinity of the side wall. This phenomenon is typical of all OWFFs. From Fig. 4a, it is obvious that the high CO concentration (>3%, in volume) in the burner region extended from the center to the side wall of the

Table 5 Comparison of the calculated and measured gas properties at the furnace exit

Parameter	Value	
	Calculation	Measurement
Gas temperature (K)	1266	1284[a]
O_2 concentration in dry gas (in volume) (%)	2.08	1.99[b]
Carbon content in fly ash (in weight) (%)	3.23	3.34

[a] Design value provided by the power plant operator; [b] Measured value obtained from the economizer exit

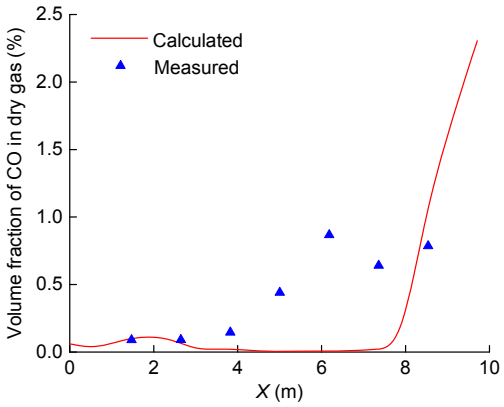

Fig. 3 Comparison of measured and calculated CO concentrations (%, in volume) along the furnace width

furnace, with the establishment of three significant peaks. Here, the high CO concentrations represented CO volume fractions in excess of 3%, the level which is generally accepted as creating a strong reducing atmosphere for high-temperature corrosion (Yang et al., 2017). The first two peaks appeared in the central part of the furnace, related to the flames emitted from the upper burners on the front wall, while the third was near the central side wall, caused by the gas from the lower part of the furnace. About four fifths of the side wall was covered by a high concentration of CO. With the injection of OFA, the overall CO level was drastically reduced, and the concentration in the furnace heart dropped to nearly zero (Fig. 4b). Yet in the OFA region, the high CO concentration (>3%, in volume) near the side wall as well as the peak around its center remained. High CO concentrations gradually formed at the front and rear walls. As a result, a U-shaped distribution of CO concentration formed along the furnace width. This trend is in line with the results from Fig. 3, suggesting that the CO distribution characteristics along the furnace width can be qualitatively analyzed by monitoring the profiles of

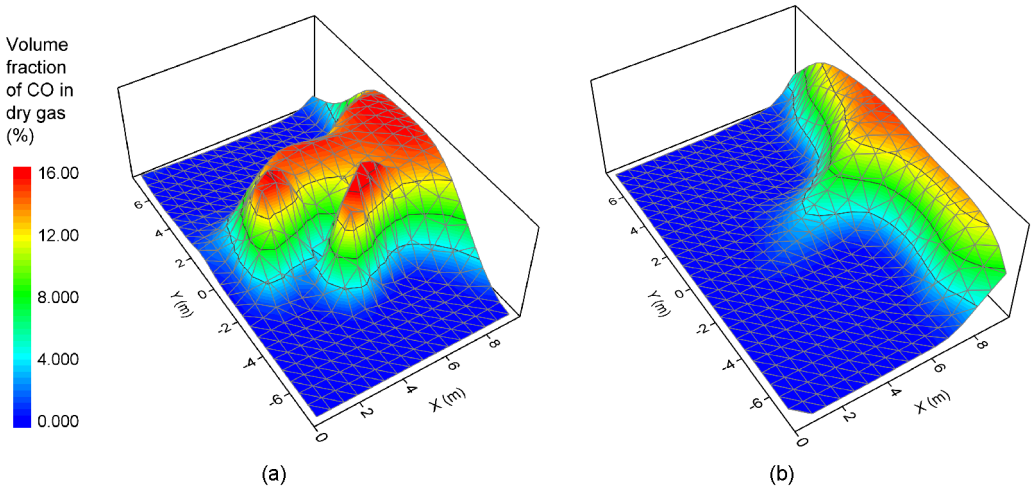

Fig. 4 Contours of CO concentration (%, in volume) at the outlets of the burner region (a) and the OFA region (b)

CO concentration in a horizontal pass or even in a vertical pass, which has been extensively confirmed and applied in industry (Hong et al., 2012; Yang et al., 2015; Xie et al., 2019).

When the OFA was introduced into the furnace, the peak value of CO concentration in the side wall region showed a slight decrease from 16.0% to 15.1% (in volume). The ratio of the zone with CO concentration >3% (in volume) to the whole cross-section area shrank from 37.8% to 22.8%. Apparently, this OFA configuration can achieve a remarkable reduction of the CO level in the furnace center, but only a weak reduction near the side wall. This is probably due to the poor mixing between the OFA and the up gas flow in the side wall region. The specific reasons for the CO distributions on these planes will be discussed later.

3.3 Correlation analysis of mixing coefficient and CO concentration distributions

A high CO concentration in the flue gas is indicative of incomplete chemical combustion, which is closely associated with the mixing of PC and air (Luo et al., 2015). Fig. 5 presents the contour of the mixing coefficient η on the planes of interest. The distribution of η at the outlet of the burner region exhibited several peaks (Fig. 5a). A high magnitude of η (>1) occupied the center of furnace and more than half of the side wall. The reason why η>1 was chosen as the criterion here is that it corresponds to the condition where the percentage of coal distributed is higher than that of air. After the addition of OFA, the values of η in the furnace center dropped and flattened out, both to a great degree (Fig. 5b). Only in the side wall region did the peaks remain visible. The high magnitude of η (>1) had progressively spread over the whole side wall. Consequently, the distribution of η showed a U-shaped profile along the furnace width. By correlating Figs. 4 and 5, it was evident that the CO concentration and η varied in roughly the same manner whilst η showed large oscillation. The oscillation resulted mainly from the non-continuous distribution of coal particles, which reflected the inherent nature of the discrete phase. The correlation coefficients between the CO concentration and η were then calculated: 0.81 for the burner and 0.87 for the OFA outlet regions. In summary, the CO concentration and η were positively correlated.

Here, an attempt was made to interpret the relationship between η and CO concentrations. According to its definition, η determines the relative sizes of PC and air distributions. When η>1, a local fuel-rich condition results. The more η surpasses 1, the denser the mass loading of coal particles and hence the more air is needed for complete combustion. However, when the O_2 concentration of the fuel-rich zone is lower, the burning process is weakened. This is conducive to CO formation, but detrimental to its oxidation, thereby resulting in a much higher CO concentration. In contrast, when η<1, the local condition is rich in O_2. Then, as η decreases, the oversupply of air increases. Drawing on the same principle, an environment of higher O_2 concentration will not only encourage the strengthened burnout,

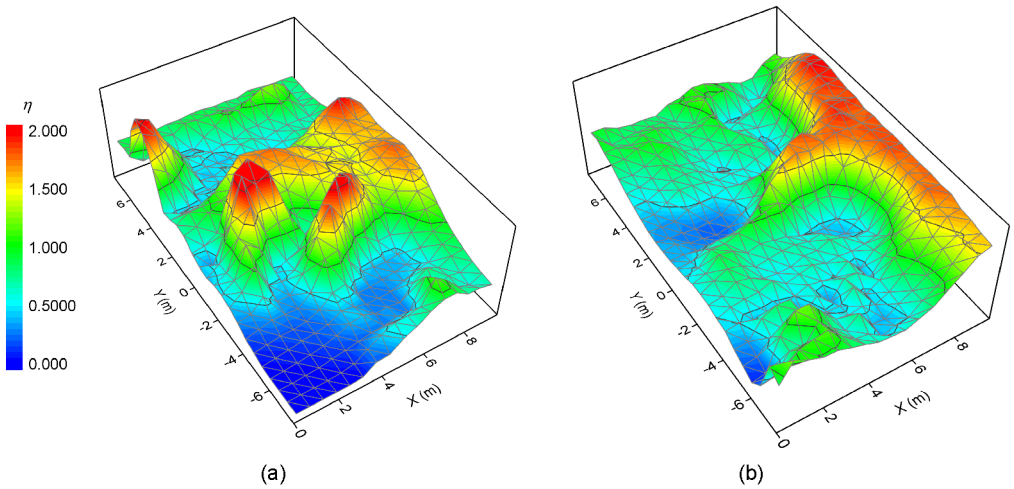

Fig. 5 Contours of the mixing coefficient η at the outlets of the burner region (a) and the OFA region (b)

inhibiting the generation of CO, but also enhance more conversion of CO to CO_2, which eventually enables the curtailment of the local CO level. In this way, larger η magnitudes monotonically lead to higher CO concentrations for the same cross-section.

3.4 Contribution of coal and air distributions to the mixing characteristics

From the previous statements, it is clear that the distribution of coal, together with that of air, plays a determinant role in fuel-air mixing, so here we focus on their respective impact on the mixing characteristics that prevail in different parts of the furnace.

Fig. 6 shows the variation in the air distribution coefficient η_a on the outlet planes of the burner and OFA regions. The air distributions were almost the same at the two cross-sections: a large quantity of air gathered in the heart of the furnace and stretching to the side walls. Viewed as a whole, the variations of η_a were insignificant across the width and height of the furnace, revealing a well-developed flame-filled furnace. This is attributable to the equal distribution of inlet streams assumed in the simulation, and the self-compensating effect of turbulent flow induced by the instantaneous fluctuations.

Fig. 7 shows the variation in the coal distribution coefficient η_p on the same cross-sections. In the burner region, a large fraction of particles was concentrated from the furnace center to the side wall. As the gas crept up to the OFA region, the particles near the side wall became further condensed and were transported downstream. In the central part of furnace, η_p values of nearly zero were reached. Sequentially, the PC has realized a distribution that is rich near the side wall and lean in the center of the furnace.

Together, Figs. 6 and 7 show that both the gas and particles had a tendency to shift towards the side wall, which shows that the movement of the gas lagged far behind that of the particles, particularly after the OFA was introduced into the furnace. As a consequence, a U-shaped distribution of particles formed along the furnace width, while the gas showed a relatively uniform distribution. This inconsistency between gas and particles movements was found to be useful as the spatial mismatch between coal and air causes heterogeneity of combustion, thus creating deviations in CO concentration. Moreover, in terms of distribution patterns, the profiles of coal particles (η_p) (Fig. 7), were globally identical to those of the mixing coefficient (η) (Fig. 5). Therefore, we conclude that, for this furnace, it is the coal that has the most effect on the mixing characteristics of PC and air. Finally, note that the OFA jet exerted a more pronounced impact on the redistribution of coal than that of air. This is possibly because the OFA stream preferentially fills the center region of the furnace, forcing the upward flue gas, laden with a considerable number of particles, outward to the side wall.

3.5 Analysis of the aerodynamic mechanism behind the formation of the CO distribution

As discussed earlier, variation in the CO concentration is thought to be caused by differences in

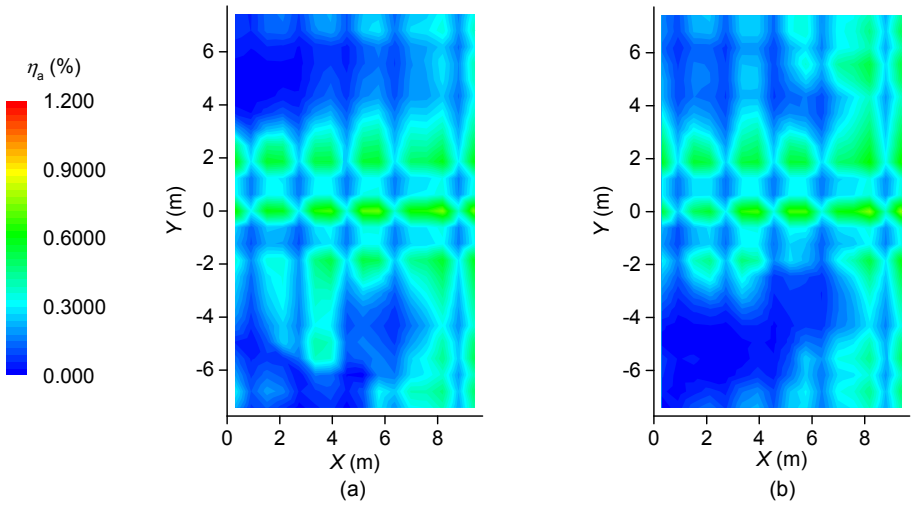

Fig. 6 Comparison of variation in the air distribution coefficient η_a at the outlets of the burner region (a) and the OFA region (b)

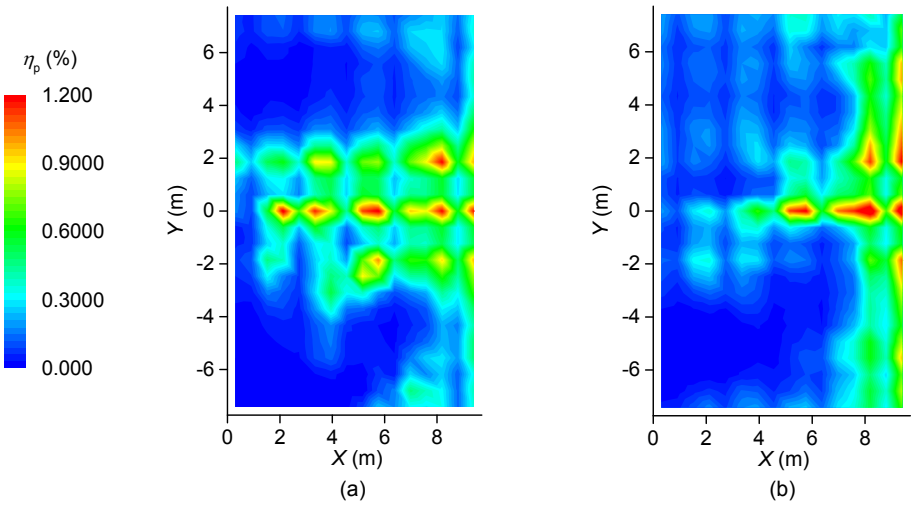

Fig. 7 Comparison of variation in the coal distribution coefficient η_p at the outlets of the burner region (a) and the OFA region (b)

the aerodynamic behavior of gas and particles. For this reason, specific analyses of the aerodynamic fields in different parts of the furnace were carried out, and the mechanisms determining how the flow regimes influence the CO distributions were revealed.

Fig. 8 depicts the streamlines of flue gas superimposed on the contour of the O_2 concentration at the cross-sections passing from the main burners. The gas flow injected from the burner initially collided with its opposite flow in the furnace center, and then deflected to the side wall. Later, it swept along the furnace until being entrained by the SA from the burner adjoining the side wall. Thus, a moderate vortex was developed at each corner of the furnace. Also, the gas tended to move toward the side walls. This phenomenon can be explained as follows: the collision of opposite flows in the center of furnace created a fairly high distribution of gas (Fig. 6a) and also a high pressure area, which pushed the gas to the side wall.

In the burner region, although the combustion air and PC were injected synchronously into the furnace, the distribution of coal particles was less uniform than that of air (Figs. 6a and 7a), which implies that the particle jet diverged from the gas jet in the course of flowing. The collision of opposite

flows in the middle of the furnace and the vortexes at the corners which characterize the flow field in the burner region, and the larger inertia of the dispersed phase, are responsible for the concentration of most particles along the furnace center to the central side wall, where the fluid velocity and direction change markedly. Once particles approach the side wall region, they will be easily thrown out of the corner vortex under the centrifugation effects, and will then adhere to the side wall because of friction with the solid surfaces. These results indicate that the mass loading of particles stuck in the vicinity of the side wall will increase continuously, as the flue gas spirals up to the outlet of the burner region, which in turn makes mixing with OFA potentially more difficult in the later stage.

When the PC enters the furnace, devolatilization takes place quickly due to the high temperatures and kinetic rates of volatile release (Karampinis et al., 2012). The volatiles burn intensively in this early combustion stage, with high O_2 consumption. In this way, the O_2 is exhausted to below 1% (in volume) in the center and in the side wall region (Fig. 8). Once the volatiles are fully burnt and the char begins to ignite, an oxygen-depleted atmosphere is formed in these zones. The residual char particles become concentrated and combust under this oxygen-depleted condition, therefore contributing to a great deal of simultaneous CO formation. All of these factors lead to the presence of a high CO concentration along the furnace center to the side wall (Fig. 4a).

Fig. 9 presents the pathlines for the main OFA port and the side OFA port. The jets from main OFA port penetrated deeply, and then flew up to the furnace exit. Some of the pathlines collided in the middle of the furnace, thus creating no gaps between the OFA jets. This was caused by both the high rates of main OFA streams and the large upward momentum of gas from the burner region. In contrast, due to the lower flow rates, the side OFA jets traveled directly upward and were adjacent to the front or rear wall. Note that although the main OFA ports are in the same arrangement as the swirl burners (Fig. 1), the main OFA jets did not follow the tendency of diffusion toward the side wall. The reason is that without being impeded by the jets from a higher level, the main OFA streams moved up along the center of the furnace. In particular, the side OFA streams rushed straight to the center of the furnace. This is because the air distribution close to the front and rear walls is quite low in the middle (Fig. 6b), as is the pressure, thus inhaling the side OFA jets nearby.

As only the burnout air is supplied into the OFA region, the mixing quality of the air and upward flue gas is the factor that determines the CO distribution in this region. Compared with the burner region, the PC was more concentrated near the side wall in the

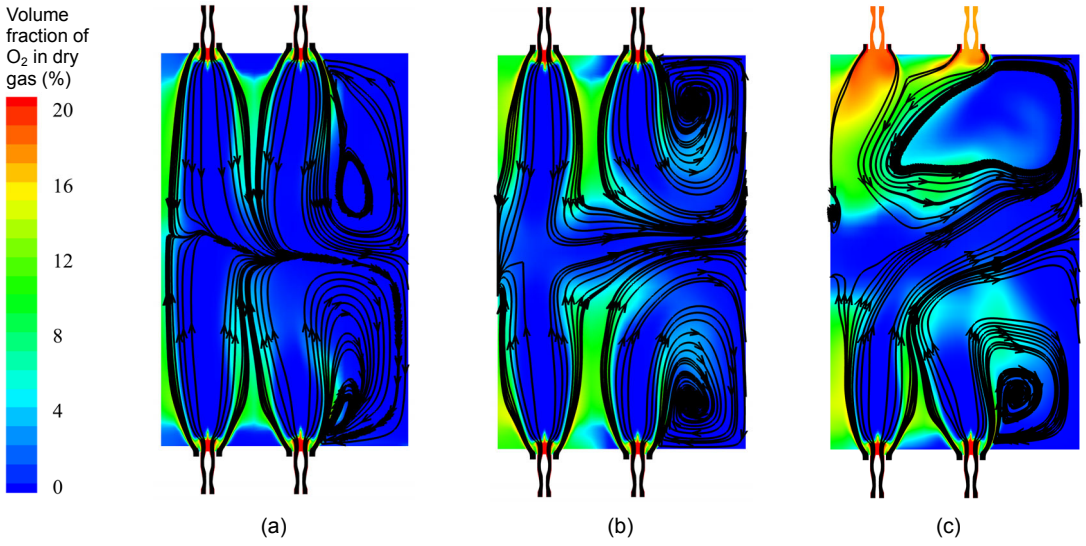

Fig. 8 Streamlines of gas flow and distributions of O_2 concentration (%, in volume) over cross-sections through the centers of the lower burners (a), the middle burners (b), and the upper burners (c)

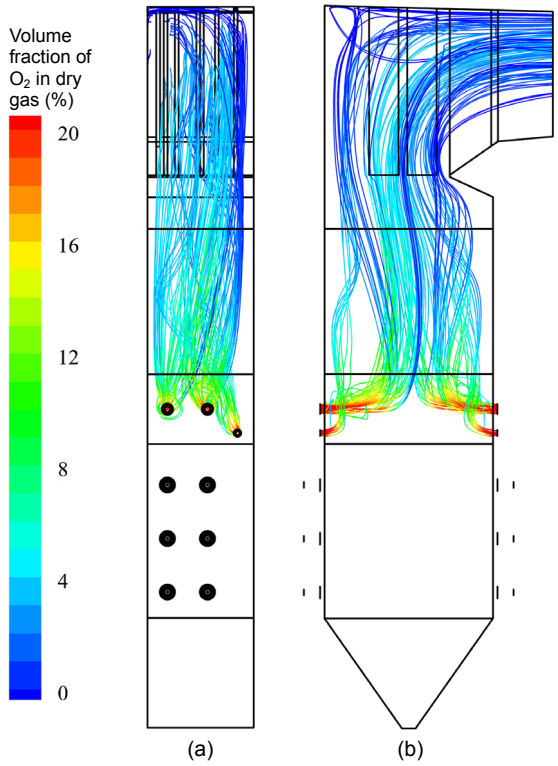

Fig. 9 Pathlines of OFA streams (colored as a function of the O_2 concentration, in volume) in front view (a) and side view (b)

OFA region, whereas the air distribution showed no significant changes (Figs. 6 and 7). Thus, the match between the air and coal worsened, which shows that there was poor mixing between the OFA and upward flue gas, especially in the side wall region. With the injection of OFA, the fresh air occupied the central region of the furnace and drove the gas from the underside outward to the side wall. As a result, most particles were dragged in proximate to the side wall. These features further increased the variation in the CO concentration in the furnace. On the one hand, the surplus char and CO concentrations in the center of the furnace are greatly reduced because of dilution and oxidization by the OFA. On the other hand, a large amount of char and CO is resident in the vicinity of the side wall, and does not mix with the OFA. Therefore, the reburning of combustibles is weakened, and a relatively high concentration of CO is maintained. This is why a U-shaped distribution of CO forms with a low concentration in the middle of the furnace and a high concentration near the side wall.

3.6 Analysis of methods to control variation in CO concentration

In engineering practice, two main methods have been used to ease the variation in CO concentration: (1) enhancing the bowl-shaped air distribution between burners and OFA ports (Xie et al., 2019); (2) incorporating side OFA ports into the combustion system, as in this study. The principle of these approaches is to send more fresh air to the periphery of the side wall where most char particles are distributed, while ensuring a proper balance between air and coal. Although both measures have certain effects on lowering the CO concentration near the side wall, they are not able to resolve the problem at its root. From the above discussion, we conclude that the vortexes formed in the corners of the furnace and the inefficient mixing capacity of OFA in the side wall region are two critical causes of the U-shaped distribution of CO concentration along the width of the furnace. Therefore, the variation in CO concentration could be reduced by decreasing the corner vortexes and strengthening the mixing of OFA and upward flue gas. With this aim in mind, we propose a patented side air technology. A set of side air nozzles is installed at the same elevations as the burners and main OFA ports, and close to the side walls, from which air with high momentum is injected counter to the swirling direction of the corner vortex, thereby suppressing the corner vortexes. Furthermore, the newly added side air intensifies the mixing of fresh air and upward flue gas in the side wall region. Detailed analyses of this scheme await future studies.

4 Conclusions

The spatial distributions of coal and air, and the mixing and flow characteristics of a 660 MW OWFF were investigated numerically, with an emphasis on the causes of variation in the CO distribution along the furnace width. Based on the simulation, we conclude that:

1. The CO distribution within the furnace is characterized by a high concentration near the side wall and a low concentration in the middle. Closer examination showed that, in the burner region, CO is concentrated along the furnace center to the side wall,

while after the injection of OFA, most of the CO is attached to the side wall.

2. The consistency between the distributions of CO concentration and η indicates that the mixing characteristics of coal and air are of critical importance to the formation of the CO distribution. Non-uniform mixing characteristics lead to an uneven combustion process, resulting in the observed variation in CO concentration.

3. A comparison of η_a and η_p showed that although both the gas and particles were inclined to flow to the side wall, the particles could reach the side wall more easily. As a result, the air showed a relatively uniform distribution, while the coal was more concentrated in the vicinity of the side wall.

4. In the burner region, the collision between opposite flows pushed the gas and particles to the side wall. Then a moderate vortex was formed in each corner of furnace, which further trapped the particles in the side wall region. In this way, a large fraction of the char was concentrated and oxygenized along the furnace center to the side wall, which produced a great amount of CO.

5. As the OFA jet was injected into the furnace, it preferentially filled the central part of the furnace and sent the gas from the underside of the furnace outward to the side wall. This implies that the mixing capacity of OFA was weak in the side wall region, which is disadvantageous for reducing CO. Consequently, a so-called U-shaped distribution of CO was formed.

6. The purpose of a side OFA is to supplement the fresh air to the side wall, but due to the low flow rates, the air does not flow along the side wall as expected.

7. All the features stated above demonstrate that the vortexes formed in the furnace corners and the deficient mixing capacity of OFA in the side wall region are two critical causes of the U-shaped distribution of CO concentration along the width of the furnace. In view of these results, the adoption of side air technology is recommended.

Contributors

Jian-guo YANG, Chao-yang ZHU, and Hong ZHAO proposed the research goal. Jian-guo YANG and Xiao-qiang XIE designed the research. Xiao-qiang XIE conducted the research and analyzed the corresponding data. Chao-yang ZHU and Chuan-huai LIU provided the technical assistance during the in-situ experiment. Xiao-qiang XIE wrote the first draft of the manuscript. Jian-guo YANG and Hong ZHAO helped to organize and revise the manuscript. Zhi-hua WANG offered valuable guidance for the fulfillment of the manuscript. Xiao-qiang XIE revised and edited the final version.

Conflict of interest

Xiao-qiang XIE, Jian-guo YANG, Chao-yang ZHU, Chuan-huai LIU, Hong ZHAO, and Zhi-hua WANG declare that they have no conflict of interest.

References

Bar-Ziv E, Saveliev R, Korytnyi E, et al., 2014. Evaluation of performance of Anglo-Mafube bituminous South African coal in 550 MW opposite-wall and 575 MW tangential-fired utility boilers. *Fuel Processing Technology*, 123: 92-106. https://doi.org/10.1016/j.fuproc.2014.01.026

Baum MM, Street PJ, 1971. Predicting the combustion behaviour of coal particles. *Combustion Science and Technology*, 3(5):231-243. https://doi.org/10.1080/00102207108952290

Chen XD, Kong LX, Bai J, et al., 2017. Study on fusibility of coal ash rich in sodium and sulfur by synthetic ash under different atmospheres. *Fuel*, 202:175-183. https://doi.org/10.1016/j.fuel.2017.04.001

Chen ZC, Li ZQ, Jing JP, et al., 2008. The influence of fuel bias in the primary air duct on the gas/particle flow characteristics near the swirl burner region. *Fuel Processing Technology*, 89(10):958-965. https://doi.org/10.1016/j.fuproc.2008.03.005

Chen ZC, Li ZQ, Zhu QY, et al., 2011. Gas/particle flow and combustion characteristics and NO_x emissions of a new swirl coal burner. *Energy*, 36(2):709-723. https://doi.org/10.1016/j.energy.2010.12.037

Cheng P, 1964. Two-dimensional radiating gas flow by a moment method. *AIAA Journal*, 2(9):1662-1664. https://doi.org/10.2514/3.2645

Choi CR, Kim CN, 2009. Numerical investigation on the flow, combustion and NO_x emission characteristics in a 500 MW_e tangentially fired pulverized-coal boiler. *Fuel*, 88(9):1720-1731. https://doi.org/10.1016/j.fuel.2009.04.001

Costa M, Azevedo JLT, 2007. Experimental characterization of an industrial pulverized coal-fired furnace under deep staging conditions. *Combustion Science and Technology*, 179(9):1923-1935. https://doi.org/10.1080/00102200701385042

Drosatos P, Nikolopoulos N, Agraniotis M, et al., 2016. Numerical investigation of firing concepts for a flexible Greek lignite-fired power plant. *Fuel Processing Technology*, 142:370-395. https://doi.org/10.1016/j.fuproc.2015.10.033

Fan JR, Sun P, Zheng YQ, et al., 1999. Numerical and experimental investigation on the reduction of NO_x emission in a 600 MW utility furnace by using OFA. *Fuel*, 78(12):1387-1394. https://doi.org/10.1016/S0016-2361(99)00062-9

Fan WD, Li YY, Lin ZC, et al., 2010. PDA research on a novel pulverized coal combustion technology for a large utility boiler. *Energy*, 35(5):2141-2148. https://doi.org/10.1016/j.energy.2010.01.033

Field MA, 1969. Rate of combustion of size-graded fractions of char from a low-rank coal between 1200 K and 2000 K. *Combustion and Flame*, 13(3):237-252. https://doi.org/10.1016/0010-2180(69)90002-9

He BS, Chen MQ, Liu SM, et al., 2005. Measured vorticity distributions in a model of tangentially fired furnace. *Experimental Thermal and Fluid Science*, 29(5):537-554. https://doi.org/10.1016/j.expthermflusci.2004.05.020

Hong R, Shen Y, Zhao Z, 2012. Emission characteristics of CO and NO_x from opposed firing boiler in a 600 MW supercritical unit. *Journal of Chinese Society of Power Engineering*, 32(12):922-927. https://doi.org/10.3969/j.issn.1674-7607.2012.12.003

Huang LK, Li ZQ, Sun R, et al., 2006. Numerical study on the effect of the over-fire-air to the air flow and coal combustion in a 670 t/h wall-fired boiler. *Fuel Processing Technology*, 87(4):363-371. https://doi.org/10.1016/j.fuproc.2005.10.008

Karampinis E, Nikolopoulos N, Nikolopoulos A, et al., 2012. Numerical investigation Greek lignite/cardoon co-firing in a tangentially fired furnace. *Applied Energy*, 97:514-524. https://doi.org/10.1016/j.apenergy.2011.12.032

Kobayashi H, Howard JB, Sarofim AF, 1977. Coal devolatilization at high temperatures. *Symposium (International) on Combustion*, 16(1):411-425. https://doi.org/10.1016/S0082-0784(77)80341-X

Li ZQ, Sun R, Chen LZ, et al., 2002. Effect of primary air flow types on particle distributions in the near swirl burner region. *Fuel*, 81(6):829-835. https://doi.org/10.1016/S0016-2361(01)00179-X

Li ZQ, Jing JP, Chen ZC, et al., 2008. Combustion characteristics and NO_x emissions of two kinds of swirl burners in a 300-MW_e wall-fired pulverized-coal utility boiler. *Combustion Science and Technology*, 180(7):1370-1394. https://doi.org/10.1080/00102200802043318

Li ZQ, Li S, Zhu QY, et al., 2014. Effects of particle concentration variation in the primary air duct on combustion characteristics and NO_x emissions in a 0.5-MW test facility with pulverized coal swirl burners. *Applied Thermal Engineering*, 73(1):859-868. https://doi.org/10.1016/j.applthermaleng.2014.08.041

Liu C, Zhao H, Yang WY, et al., 2018. Chemical kinetics simulation of semi-dry dechlorination in coal-fired flue gas. *Journal of Zhejiang University-SCIENCE A (Applied Physics & Engineering)*, 19(2):148-157. https://doi.org/10.1631/jzus.A1600653

Liu H, Liu YH, Yi GZ, et al., 2013. Effects of air staging conditions on the combustion and NO_x emission characteristics in a 600 MW wall fired utility boiler using lean coal. *Energy & Fuels*, 27(10):5831-5840. https://doi.org/10.1021/ef401354g

Luo R, Fu JP, Li N, et al., 2015. Combined control of secondary air flaring angle of burner and air distribution for opposed-firing coal combustion. *Applied Thermal Engineering*, 79:44-53. https://doi.org/10.1016/j.applthermaleng.2015.01.008

Park S, Kim JA, Ryu C, et al., 2013. Combustion and heat transfer characteristics of oxy-coal combustion in a 100 MW_e front-wall-fired furnace. *Fuel*, 106:718-729. https://doi.org/10.1016/j.fuel.2012.11.001

Purimetla A, Cui J, 2009. CFD studies on burner secondary airflow. *Applied Mathematical Modelling*, 33(2):1126-1140. https://doi.org/10.1016/j.apm.2008.01.007

Rosin P, Rammler E, 1933. The laws governing the fineness of powdered coal. *Journal of the Institute of Fuel*, 7:29-36.

Shih TH, Liou WW, Shabbir A, et al., 1995. A new k-ϵ eddy viscosity model for high Reynolds number turbulent flows. *Computers & Fluids*, 24(3):227-238. https://doi.org/10.1016/0045-7930(94)00032-T

Sivathanu YR, Faeth GM, 1990. Generalized state relationships for scalar properties in nonpremixed hydrocarbon/air flames. *Combustion and Flame*, 82(2):211-230. https://doi.org/10.1016/0010-2180(90)90099-D

Smith TF, Shen ZF, Friedman JN, 1982. Evaluation of coefficients for the weighted sum of gray gases model. *Journal of Heat Transfer*, 104(4):602-608. https://doi.org/10.1115/1.3245174

Szuhánszki J, Black S, Pranzitelli A, et al., 2013. Evaluation of the performance of a power plant boiler firing coal, biomass and a blend under oxy-fuel conditions as a CO_2 capture technique. *Energy Procedia*, 37:1413-1422. https://doi.org/10.1016/j.egypro.2013.06.017

van der Lans RP, Glarborg P, Dam-Johansen K, 1997. Influence of process parameters on nitrogen oxide formation in pulverized coal burners. *Progress in Energy and Combustion Science*, 23(4):349-377. https://doi.org/10.1016/S0360-1285(97)00012-9

Vikhansky A, Bar-Ziv E, Chudnovsky B, et al., 2004. Measurements and numerical simulations for optimization of the combustion process in a utility boiler. *International Journal of Energy Research*, 28(5):391-401. https://doi.org/10.1002/er.971

Vuthaluru R, Vuthaluru HB, 2006. Modelling of a wall fired furnace for different operating conditions using FLUENT. *Fuel Processing Technology*, 87(7):633-639. https://doi.org/10.1016/j.fuproc.2006.01.004

Xie XQ, Yang JG, Zhu CY, et al., 2019. Effect of bowl-shaped

secondary air distribution on combustion efficiency and NO_x mass concentration. *Journal of Zhejiang University (Engineering Science)*, 53(2):220-227 (in Chinese). https://doi.org/10.3785/j.issn.1008-973X.2019.02.003

Xu MH, Yuan JW, Ding SF, et al., 1998. Simulation of the gas temperature deviation in large-scale tangential coal fired utility boilers. *Computer Methods in Applied Mechanics and Engineering*, 155(3-4):369-380. https://doi.org/10.1016/S0045-7825(97)00196-5

Yang JH, Kim JEA, Hong J, et al., 2015. Effects of detailed operating parameters on combustion in two 500-MWe coal-fired boilers of an identical design. *Fuel*, 144:145-156. https://doi.org/10.1016/j.fuel.2014.12.017

Yang WJ, You RZ, Wang ZH, et al., 2017. Effects of near-wall air application in a pulverized-coal 300 MW_e utility boiler on combustion and corrosive gases. *Energy & Fuels*, 31(9):10075-10081. https://doi.org/10.1021/acs.energyfuels.7b01476

Zhou H, Yang Y, Dong K, et al., 2014. Influence of the gas particle flow characteristics of a low-NO_x swirl burner on the formation of high temperature corrosion. *Fuel*, 134: 595-602. https://doi.org/10.1016/j.fuel.2014.06.027

中文概要

题　目：前后墙对冲燃烧锅炉内 CO 分布原因的数值分析

目　的：前后墙对冲燃烧锅炉在实际运行中普遍存在沿炉膛宽度 CO 体积分数呈中间低、两边高的分布特点。该分布特点往往伴随着锅炉效率降低、炉膛出口 NO_x 排放偏高、侧墙结渣和高温腐蚀严重等一系列问题。本文旨在分析前后墙对冲燃烧锅炉内 CO 分布规律的形成原因，为机组运行调整与燃烧系统改造等工程实践提供理论依据。

创新点：1. 针对煤粉炉燃烧过程中存在剧烈气固反应流的特点，定义了与气、固相质量变化无关的风、煤分布系数 η_a 和 η_p，进而得到了风/煤混合系数 η。2. 对比炉膛不同区域内的 CO 分布与风/煤混合系数分布，结合炉膛的空气动力学特性，解释了前后墙对冲燃烧锅炉内 CO 分布特征的形成过程。

方　法：1. 建立一台 660 MWe 前后墙对冲燃烧锅炉的数值模型，并通过现场测量数据与模拟数据的比较，验证模型的有效性（表 5 和图 3）。2. 定义炉内风、煤分布系数与风/煤混合系数（公式（1）~（3））。3. 对比不同特征截面上 CO 分布特性与风/煤混合特性，探讨二者之间的关联性（图 4 和 5）。3. 分析风的分布和煤的分布分别对风/煤混合特性的影响（图 6 和 7）。4. 综合考虑炉内气流结构、风和煤的分布及其混合特性，揭示炉内 CO 分布规律的形成原因（图 4~9）。

结　论：1. 对前后墙对冲燃烧锅炉而言，燃烧器区域出口的 CO 大量聚集在炉膛中间至侧墙区域，燃尽风区域出口的 CO 则主要集中于侧墙附近。2. CO 分布与风/煤混合系数分布基本一致。3. 在整个炉膛空间内，风和煤粉皆有向侧墙流动的趋势，但煤粉更加聚集在侧墙周围。4. 在燃烧器区域，对冲气流使得风与煤粉向侧墙流动，然后在炉膛四角形成涡流；四角涡流导致烟气在沿侧墙上升的过程中发生明显的气固分离，使煤粉被甩至侧墙附近并在那里燃烧，形成高浓度 CO；5. 在燃尽风区域，燃尽风与侧墙附近烟气的混合并不理想，因此侧墙附近的高浓度 CO 难以消除，最终导致沿炉膛宽度的 CO 体积分数呈中间低、两边高的分布特点。6. 基于上述结果，本文分析了当前应用中存在的问题，并提出了改进建议。

关键词：前后墙对冲燃烧锅炉；CO 分布；风、煤分布；两相流；四角涡流；燃尽风